Dynamics of H−2 and C2H4 elimination in the Y+C2H6 reaction

4 AUTHORS, INCLUDING:

Hans U Stauffer
Wright-Patterson Air Force Base

43 PUBLICATIONS   **593** CITATIONS

Dynamics of H_2 and C_2H_4 Elimination in the $Y + C_2H_6$ Reaction

Hans U. Stauffer, Ryan Z. Hinrichs, Jonathan J. Schroden, and H. Floyd Davis*

Department of Chemistry and Chemical Biology, Baker Laboratory, Cornell University, Ithaca, New York 14853-1301

The reaction between ground-state atomic yttrium (a^2D_J) and ethane (C_2H_6) has been studied in crossed molecular beams with 157 nm photoionization detection of products. Studies have been carried out at several collision energies, ranging from $\langle E_{coll} \rangle = 16.1$ kcal/mol to $\langle E_{coll} \rangle = 29.8$ kcal/mol. At $\langle E_{coll} \rangle \geq 18.1$ kcal/mol, reactive scattering is observed, with both $YH_2 + C_2H_4$ and $YC_2H_4 + H_2$ products being formed. Detected products of the $YH_2 + C_2H_4$ channel are found to exhibit very little translational energy, suggesting that there is little or no potential energy barrier above the final product energy to ethylene elimination from an $(H)_2Y(C_2H_4)$ intermediate. Translational energy distributions for the $YC_2H_4 + H_2$ channel, resulting from elimination of H_2 from a common intermediate, demonstrate that a slightly larger fraction of energy available to these products is channeled into translation. The $YH_2 + C_2H_4$ channel is found to dominate the H_2 elimination channel by greater than an order of magnitude, which suggests that a small potential energy barrier to the less endoergic H_2 elimination channel exists. In lower collision energy studies, only nonreactive scattering of Y atoms from ethane is found to occur. This observed collision energy threshold behavior for the onset of YH_2 and YC_2H_4 product formation allows determination of the barrier to C−H bond insertion of Y atoms into ethane to be 19.9 ± 3.0 kcal/mol.

I. Introduction

Experimentally, recent years have brought significant advances in the ability of researchers to study the interactions of hydrocarbon molecules, both saturated and unsaturated, with neutral transition metal atoms in the gas phase. Initial kinetics studies of these types of reactions have relied solely on probes of the metal atom reactant depletion, using either flow tube[1−12] or laser photolysis−laser fluorescence[13−20] techniques to gain insight into the rate constants of metal atom−hydrocarbon reactions for a broad series of reactants. In conjunction with theoretical calculations, the measured rate constants were justified and the bimolecular reaction products or stabilized termolecular reaction complexes of these reactions could be inferred. More recently, experimental techniques utilizing 157 nm photoionization[21−24] or electron impact ionization[25] detection have allowed direct observation of the bimolecular reaction products formed from a small subset of these reactions.

In the previous studies, observed or inferred bimolecular reaction products from neutral metal atom−hydrocarbon reactions have been largely limited to those products resulting from reductive elimination of H_2 from reaction intermediates.[5−7,21−25] Indeed, for most reactions studied thus far, molecular hydrogen elimination is the energetically favored bimolecular reaction pathway and is therefore most readily observed. In some cases, however, other interesting reactive pathways lie relatively low in energy and can therefore be studied at slightly larger collision energies where competition can exist between H_2 elimination and other reactive pathways. This is, for example, the case in the reaction between Y atoms and ethane, C_2H_6, where $YC_2H_4 + H_2$ formation is the most energetically favorable product channel, calculated to lie 5.0 kcal/mol endoergic to the reactant

   * To whom correspondence should be addressed. E-mail: HFD1@cornell.edu.

asymptote and driven predominantly by the formation of a strongly bound YC_2H_4 adduct.[5] However, a second product channel, resulting in $YH_2 + C_2H_4$ products, is expected to be only slightly less thermodynamically favorable, owing to the formation of two relatively strong M−H bonds in YH_2.[26,27] This ethylene elimination channel from the initial insertion intermediate is particularly interesting in that the reverse reaction, i.e., 1,2-insertion of an alkene into a metal hydride bond to form a transition metal alkyl species, plays a key role in a variety of catalytic reactions, including alkene hydrogenation, alkene isomerization, and alkene hydroformylation.[28]

To ultimately eliminate these molecular species, the yttrium atom must initially insert into an ethane C−H bond to form the HYC_2H_5 oxidative addition products. Such oxidative addition processes of alkanes to coordinatively and electronically unsaturated transition metal centers play an important role in the conversion of largely nonreactive alkanes to more reactive species, and as such, have garnered considerable experimental and theoretical attention over the past few decades, as reviewed extensively by several authors.[29,30] Recently, a series of theoretical calculations, primarily focusing on reactions of bare second-row transition metal atoms, have demonstrated that potential energy barriers to C−H insertion into alkanes by transition metal atoms are due predominantly to a repulsive interaction between the ground-state $d^{n-2}s^2$ or high-spin $d^{n-1}s^1$ electronic configurations of most metal atoms and the directional sp^3 hybridized C−H σ-bond.[5,30−32] Note that similar trends in barrier heights for insertion into H_2 are expected to result from these electronic requirements, although reduced in magnitude because of the spherical nature of H atom s-orbitals, which can readily participate in multicenter bonding.[30] Thus, calculated barrier heights for oxidative addition are closely related to the promotion energies necessary to access low-spin $d^{n-1}s^1$ or d^ns^0 electronic configurations that reduce this repulsion.[5,30−32] These
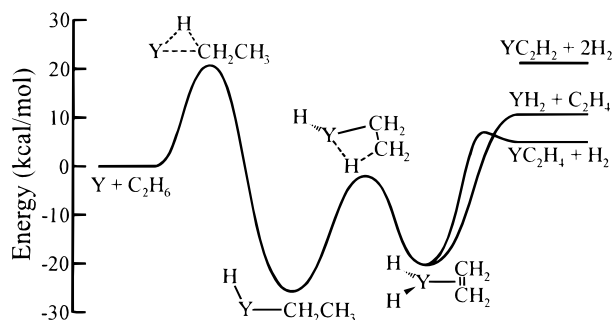
Figure 1. Schematic potential energy diagram for the Y + C_2H_6 reaction.

promotion energies, and therefore, C−H insertion barrier heights, are particularly large for early transition metal atoms such as yttrium. Since most previous experiments have been carried out at relatively low temperatures (<630 K) using thermal distributions, the accuracy of the calculated energetics for even these simple transition metal atom reactions with small alkanes is still largely untested, necessitating further comparison between experiment and theory.

We have studied reactions between ground electronic state Y atoms and C_2H_6 over a range of collision energies using the crossed molecular beams technique with 157 nm photoionization. Despite relatively small reactive cross sections expected for this reaction, 157 nm photoionization provides sufficient sensitivity to probe both reaction channels accessible at these collision energies, as well as scattered Y atoms resulting from nonreactive encounters between yttrium and ethane.[33] Detection of these three different channels is further simplified by the fact that yttrium (^{89}Y) is isotopically pure.[34] Thus, differentiation among Y, YH_2, and YC_2H_4 signals using mass spectrometry following ionization is straightforward.

A schematic potential energy diagram for the ground-state $Y(a^2D_{3/2}) + C_2H_6$ reaction showing the most likely pathway to product formation following C−H insertion is shown in Figure 1. Although the barrier to C−H insertion into ethane has not been directly calculated, the analogous transition state for the Y + CH_4 reaction is predicted to lie 20.7 kcal/mol above the reactant asymptote.[5,31] A similar barrier height is expected for this reaction; however, the barrier calculated for the Y + CH_4 reaction has been corrected for zero-point vibrational effects,[5,31] which will differ for the Y + C_2H_6 reaction. Following formation of a C−H insertion intermediate, β-hydrogen transfer may occur resulting in the dihydrido intermediate, $(H)_2Y(C_2H_4)$. The barrier to this transfer as well as the energetics of the initial insertion complex may be stabilized relative to the energetics shown in Figure 1 because of the presence of β-agostic bonding in the insertion complex. This type of interaction, which involves transfer of electron density from the C−H$^\beta$ σ-bond to empty orbitals of the metal atom, has been found to play an important role in β-elimination from the ethyl group in $Pd(C_2H_5)(H)$-(PH_3).[35] Theoretical calculations suggest that β-agostic bonding is not present in related reactions between ethane and bare Pd and Rh,[5] both of which lie to the right of the periodic table and have nearly filled d-shells. However, such interactions may play a larger role in the Y + C_2H_6 reaction, since Y has only three valence electrons and can therefore readily accept σ-electron density from the hydrocarbon. The final dihydrido complex can eliminate either H_2 or C_2H_4 to form the two energetically accessible product channels. On the basis of the YH_2 binding energy calculated by Siegbahn,[27] the YH_2 + C_2H_4 product channel is 6 kcal/mol less favorable than the YC_2H_4 + H_2 channel, as depicted in Figure 1. In fact, earlier calculations on

YH_2 by Balasubramanian and Ravimohan (BR)[26] determined this binding energy to be substantially stronger; however, the more recent calculations suggest that BR used an inadequate effective core potential and therefore overestimated the YH_2 binding energy.[27]

II. Experiment

All experiments reported here were carried out using the crossed molecular beams apparatus described in ref 33. The Y atomic beam, prepared and characterized as discussed in a previous publication,[23] is generated by laser vaporization[36] from a 0.25 in. diameter yttrium rod (Alfa Aesar, 99.9%) at the throat of a supersonic expansion of carrier gas issuing from a piezoelectric pulsed valve.[37] The differentially pumped yttrium beam is collimated by a 0.5 mm diameter skimmer and a 2 mm × 2 mm square aperture before passing into the main chamber region maintained below 2×10^{-6} Torr. A slotted wheel (22.9 cm diameter, 0.5 mm slot) spun at 210 Hz provides additional temporal resolution of the Y atom pulse. A second pulsed valve is used to generate a beam of C_2H_6 (Matheson), seeded in H_2, that crosses the yttrium atomic beam at a fixed right angle geometry. These two beams can be rotated with respect to a fixed triply differentially pumped detector housing a quadrupole mass spectrometer and ion counting electronics. The metal atom and hydrocarbon beam velocities are measured by detecting the beam species on-axis through a 0.254 mm diameter aperture on the front of the detector using electron impact ionization, and these distributions are fit to a functional form.[33] Scattered products from Y + C_2H_6 collisions traverse a flight distance of 24.1 cm before being ionized using the 157 nm output of an F_2 laser (Lambda Physik LPX 220i). Time-of-flight (TOF) spectra of scattered products are measured by scanning the delay of the ionization laser relative to a time zero defined by the slotted wheel while counting all ionized products of a given mass-to-charge (m/e) ratio as a function of ionization laser delay. Laboratory angular distributions of scattered products are obtained by integrating TOF spectra obtained at various laboratory angles, θ, measured with respect to the Y atom beam axis.

The forward convolution technique was used to analyze the experimental data. Several known instrumental parameters (e.g., atomic and molecular beam angular widths, scattered product flight distance, detector aperture size, etc.) along with the measured beam velocity distributions are input into a Windows-based computer program. Simulated laboratory angular distributions and TOF spectra are then calculated and compared to the experimental data assuming separable input center-of-mass (c.m.) flux distributions: $P(E)$, the c.m. translation energy distribution, and $T(\Theta)$, the c.m. angular distribution. These c.m. distributions are subsequently iteratively adjusted to achieve optimal agreement between simulation and experimental data. The normalized $P(E)$ distributions are generated using a functional form[38−40] as described previously.[23]

III. Results and Analysis

In a previous publication,[23] we have detailed a characterization of the states populated in the ablated yttrium atomic beam using laser-induced fluorescence. At the molecular beam interaction volume, the Y beam is found to contain predominantly the two spin−orbit states of the ground a^2D_J (d^1s^2) electronic state, with no evidence for population of excited electronic states. There is evidence for some YO contamination in the metal atom beam; however, experiments have been carried

H$_2$ and C$_2$H$_4$ Elimination

J. Phys. Chem. A, Vol. 104, No. 6, 2000 **1109**

TABLE 1: Mean Collision Energies ($\langle E_{coll} \rangle$), Peak Velocities (v_{pk}), and fwhm of Velocity Distributions for Y + C$_2$H$_6$ Studies

|	yttrium beam			C$_2$H$_6$ beam		
$\langle E_{coll} \rangle^a$	carrier gas	v_{pk}^b	fwhm^b	beam composition	v_{pk}^b	fwhm^b
16.1	8% Ne in He	2170	300	40% in H$_2$	1140	160
18.1	8% Ne in He	2170	300	20% in H$_2$	1430	160
18.5	He	2380	360	40% in H$_2$	1140	160
20.4	8% Ne in He	2170	300	10% in H$_2$	1700	180
23.0	50% H$_2$ in He	2560	350	20% in H$_2$	1420	160
25.3	He	2420	330	8% in H$_2$	1890	180
29.8	H$_2$	3010	410	20% in H$_2$	1420	160

^{a} $\langle E_{coll} \rangle$ in kcal/mol. ^{b} Velocities in m/s.

out to determine that these impurities do not contribute to the observed reactive signal.

Reactions between yttrium atoms and C$_2$H$_6$ were studied at several collision energies ranging from $\langle E_{coll} \rangle = 16.1$ kcal/mol up to $\langle E_{coll} \rangle = 29.8$ kcal/mol by varying the compositions of the beam carrier gases. Table 1 shows the peak beam velocities, v_{pk}, and fwhm of the measured velocity distribution for each reactant at several of the collision energies studied. To achieve these relatively large collision energies using seeded molecular beams, it was necessary in some cases to use neat H$_2$ or mixtures containing H$_2$ as seed gases. It is therefore important to ensure that the observed reactive signal does not result from collisions involving YH or YH$_2$ species in the metal atom beam or collisions between species in the metal atom beam and H$_2$ molecules present in the molecular beam. To check for the presence of YH and YH$_2$ in the metal beam, the intensities observed at $m/e = 89$, 90, and 91 were compared while monitoring this beam on-axis using both electron impact ionization and 157 nm photoionization. The relative intensities observed at these masses were found to be the same using either neat H$_2$ or neat He as the metal beam seed gas. Thus, signal observed on-axis at $m/e = 90$ and 91 results only from overflow of the $m/e = 89$ signal due to imperfect mass resolution. Furthermore, both YH$_2$ and YC$_2$H$_4$ reactive signals are observed at several different collision energies, as discussed below, including collision energies in which neat He is used as the Y atom carrier gas. These observations confirm that the presence of H$_2$ in the metal atom beam is not a necessary condition for detection of reaction products. Note also that reactions of species in the metal atom beam with the H$_2$ seed gas of the molecular beam cannot contribute to the YH$_2$ signal observed at laboratory angles larger than a few degrees because the c.m. angles for Y + H$_2$ and YH + H$_2$ collisions are less than 1° for all collision energies studied here.

In the presentation of the experimental data, results from the $\langle E_{coll} \rangle = 23.0$ kcal/mol data set, which are qualitatively representative of several of the data sets studied, will be discussed in depth first. This will be followed by a brief description of the data from other collision energies.

A. $\langle E_{coll} \rangle = 23.0$ kcal/mol. Shown in Figure 2 is a canonical Newton diagram in velocity space, representing the transformation between the laboratory and c.m. frames of reference[41] for this reaction at $\langle E_{coll} \rangle = 23.0$ kcal/mol. At this collision energy, the velocity of the c.m. of the system lies at ~10° with respect to the Y atom beam. Superimposed on this diagram are circles corresponding to the maximum possible velocities in the c.m. frame of reference for the Y-containing fragment of the two reaction channels studied. On the basis of the theoretically calculated thermodynamics for the YH$_2$ + C$_2$H$_4$ channel, scattered YH$_2$ products are expected to be constrained within a
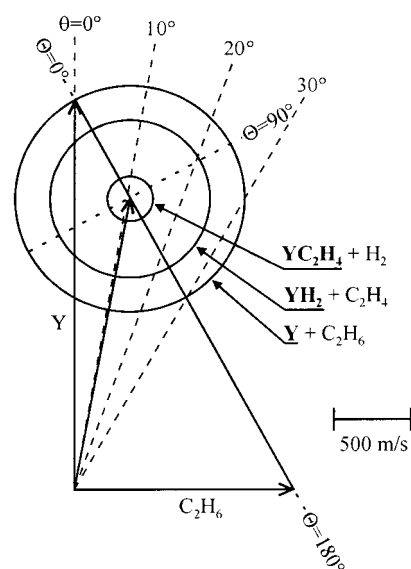
Figure 2. Newton diagram for Y + C$_2$H$_6$ collisions at $\langle E_{coll} \rangle = 23.0$ kcal/mol. Circles represent the maximum c.m. velocity constraints on the heavy fragments (shown in bold) for the various product channels based on reaction ergicity and momentum conservation.
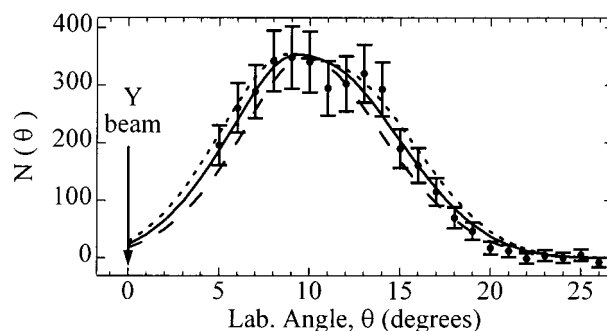

Figure 3. Measured laboratory angular distribution (closed circles) for YH$_2$ products at $\langle E_{coll} \rangle = 23.0$ kcal/mol. Solid curve is a simulation of the distribution resulting from the solid c.m. distributions shown in Figure 5, whereas dashed curves are simulations resulting from the corresponding $P(E)$ in conjunction with the solid $T(\Theta)$.

laboratory angular range $\theta = -5°$ to 26°. Despite comparable calculated energetics for the YC$_2$H$_4$ + H$_2$ channel, YC$_2$H$_4$ products are constrained to a much smaller angular range ($\theta = 6°$ to 15°) because of the lighter mass of the H$_2$ counterfragment. Also shown is a circle corresponding to elastically scattered Y atoms following collision with C$_2$H$_6$.
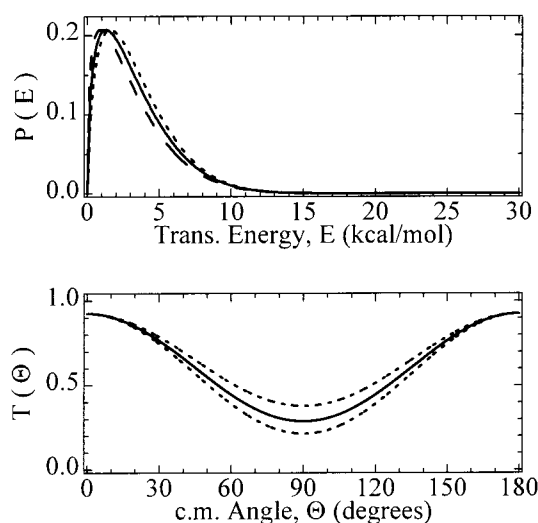
The laboratory angular distribution for YH$_2$ products, obtained at $m/e = 91$, is shown in Figure 3. This distribution has been obtained by integrating TOF spectra obtained at various laboratory angles, several of which are displayed in Figure 4. At smaller laboratory angles ($\theta < 12°$), the contribution at $m/e = 91$ from an overflow of $m/e = 89$ signal resulting from small c.m. angle scattering of Y atoms is nonnegligible, becoming increasingly important with decreasing laboratory angle. This contribution has been subtracted from the $m/e = 91$ data on the basis of the measured fractional overflow of signal from $m/e = 89$ into $m/e = 91$. At laboratory angles below ~5°, signal from forward-scattered Y atoms is large enough that this overflow can no longer be reliably subtracted from the $m/e = 91$ data.

Along with the experimental data, best-fit simulations are also included as solid curves derived using the c.m. distributions displayed in Figure 5. To simulate the experimental data properly, it is necessary to assume a dependence of the reactive
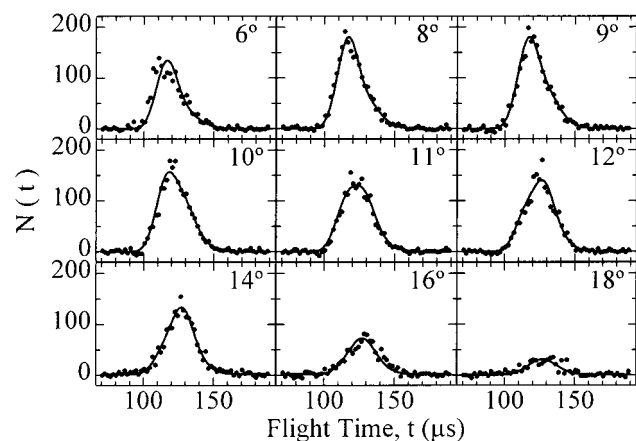
Figure 4. YH_2 product TOF spectra (solid circles) at several laboratory angles ranging from 6° to 18°. Solid curves are simulations of the experimental data resulting from the best-fit c.m. distributions shown in Figure 5.


Figure 5. Product c.m. distributions, $P(E)$ and $T(\Theta)$, for the YH_2 + C_2H_4 reaction channel at $\langle E_{coll} \rangle = 23.0$ kcal/mol. Solid curves represent distributions that best simulate laboratory angular distribution (Figure 3) and TOF spectra (Figure 4), whereas dashed curves represent the range of distributions that reasonably simulate experimental data.

cross section on the collision energy of the colliding partners. Such a dependence is not unexpected given the large calculated barrier to C−H bond insertion and the proximity of this collision energy to the calculated barrier height. In the calculation of the simulated TOF spectra and laboratory angular distribution for the YH_2 products, a simple step function probability for the reaction cross section has been assumed, corresponding to a threshold behavior of the reaction probability at a specific collision energy. The arrival times of the calculated TOF data are quite sensitive to this assumed threshold, as is expected because only the faster components of the total reactant velocity distribution will contribute to the formation of products. Without this assumed energy dependence, calculated TOF spectra at all angles peak roughly 6 μs too slow regardless of the assumed c.m. distributions. The simulations shown in Figures 3 and 4 were calculated assuming a threshold for reaction of 23.4 kcal/ mol. Changing this assumed threshold by more than approximately 0.5 kcal/mol shifts the simulated TOF enough that the calculated TOFs can no longer reasonably simulate the arrival times of the experimental data at all angles.

To estimate the uncertainty in the best-fit c.m. distributions, calculations were carried out assuming the range of $P(E)$
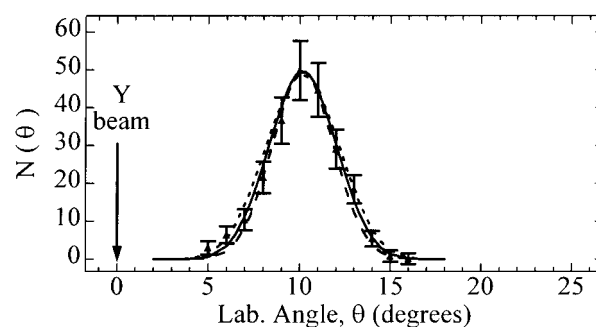
Figure 6. Laboratory angular distribution for YC_2H_4 products at $\langle E_{coll} \rangle = 23.0$ kcal/mol. Closed symbols are experimental data, whereas the solid curve is a simulation resulting from the $P(E)$ and $T(\Theta)$ shown in Figure 8.
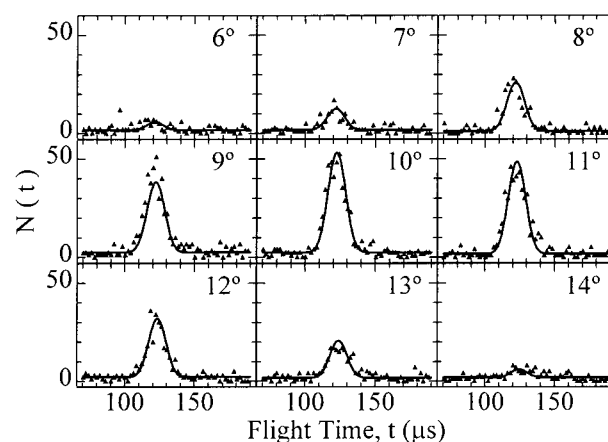

Figure 7. Measured TOF spectra (closed symbols) obtained at various laboratory angles for YC_2H_4 reaction products at $m/e = 117$. Solid curves are calculated spectra obtained using the c.m. distributions shown in Figure 8.

distributions shown as dashed curves in conjunction with the solid $T(\Theta)$ in Figure 5, still using a threshold collision energy of 23.4 kcal/mol. Calculated laboratory angular distributions using these limiting $P(E)$'s are included as dashed curves in Figure 3. Since the recoiling counterfragment for this product channel, C_2H_4, is relatively massive, the simulated TOF spectra and laboratory angular distribution are quite sensitive to small changes in the $P(E)$ and are particularly sensitive to the degree of peaking of the $P(E)$ away from zero kinetic energy. The best-fit $P(E)$ for this channel peaks at 1.3 kcal/mol, with a mean translational energy of 3.3 kcal/mol, indicating that a large fraction of energy available to this product channel exists as internal excitation of the YH_2 + C_2H_4 products.

Uncertainty ranges are also shown as dashed curves for the best-fit c.m. angular distribution, $T(\Theta)$, for the YH_2 + C_2H_4 channel. Again, owing to the heavy recoiling counterfragment for the detected YH_2 products, the simulations are quite sensitive to the form of the $T(\Theta)$ used. Most notably, the best-fit $T(\Theta)$ is forward−backward symmetric, with a substantial degree of peaking at the poles (i.e., $\Theta = 0°$ and 180°).

The YC_2H_4 products, detected at the parent $m/e = 117$, were found to be constrained to a much smaller range of laboratory angles than were the YH_2 products, as is apparent in Figure 6. As noted above, this is expected given the light mass of the H_2 counterfragment. This kinematic constraint is also evident in the TOF spectra for these products, shown in Figure 7, with YC_2H_4 products arriving over a much smaller time range compared to the YH_2 reaction products.

H$_2$ and C$_2$H$_4$ Elimination

J. Phys. Chem. A, Vol. 104, No. 6, 2000 **1111**
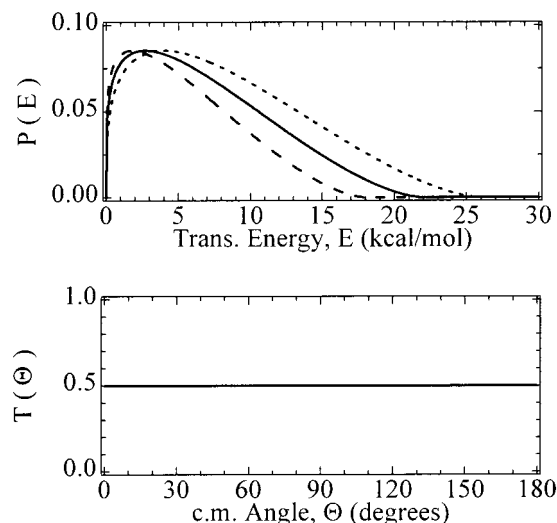
Figure 8. Product c.m. distributions for the YC$_2$H$_4$ + H$_2$ channel at $\langle E_{coll} \rangle = 23.0$ kcal/mol. Solid curves are the best-fit distributions; dashed curves represent a range of distributions giving an acceptable range of simulation.

It should be noted that at this collision energy, signal was also observed at $m/e = 115$, corresponding to YC$_2$H$_2^+$. However, the shapes of the individual TOF spectra at all angles as well as the laboratory angular distribution observed at this m/e ratio appear to exactly reproduce, within the signal-to-noise of the experimental data, the data obtained at $m/e = 117$. This $m/e = 115$ signal therefore appears to result at least to a large extent from fragmentation of YC$_2$H$_4$ reaction products to YC$_2$H$_2^+$ + H$_2$ + e$^-$ during the photoionization process. By comparison of the experimental $m/e = 117$ data to simulation, it was assumed that the extent of fragmentation of YC$_2$H$_4$ is independent of the product internal energy, justified by the fact that the signals at $m/e = 115$ and 117 appear to be identical. It is possible that some of the signal detected at $m/e = 115$ results from secondary fragmentation, prior to the photoionization process, of highly internally excited nascent YC$_2$H$_4$, since the YC$_2$H$_2$ + 2H$_2$ asymptote is calculated to lie roughly 21.2 kcal/mol above ground-state Y + C$_2$H$_6$ reactants.[5] Implications of this secondary fragmentation channel will be discussed in greater detail in section IV.

The best-fit $P(E)$ and $T(\Theta)$ distributions for the YC$_2$H$_4$ + H$_2$ product channel are shown in Figure 8. To accurately simulate the arrival times and widths of the YC$_2$H$_4$ TOF spectra, it is again necessary to assume a threshold collision energy of 23.4 kcal/mol for formation of these reaction products. Immediately evident in the best-fit $P(E)$ is a larger degree of product translational energy compared to that for the YH$_2$ + C$_2$H$_4$ channel, peaking at 2.5 kcal/mol and extending to approximately 22 kcal/mol. The mean translational energy for this product channel is found to be 7.1 kcal/mol. The best-fit c.m. angular distribution for this channel shows forward−backward symmetry and is essentially isotropic.

In addition to the two reaction product channels observed at this collision energy, signal was also observed for nonreactive scattering of Y atoms off ethane. Figure 9 shows TOF spectra for signal at $m/e = 89$ at several laboratory angles. At all angles, both fast and slow components are present in the experimental data, resulting from sampling the faster and slower edges of the Y + C$_2$H$_6$ Newton circle (Figure 2). At wider laboratory angles ($\theta > 25°$), the two components begin to coalesce into a single peak as the outer edge of the Newton circle is being sampled at these larger angles. At all angles, the faster
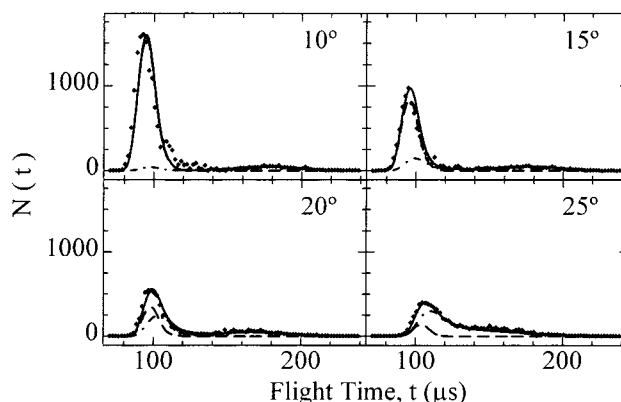

Figure 9. Nonreactively scattered Y atom TOF spectra recorded at several selected angles as shown. Simulated spectra include two components corresponding to a forward-scattered contribution (- - -) and a backward-scattered contribution (-·-).

component of the TOF is more intense than the slower component. These data therefore do not show behavior that is indicative of a strong component of backward nonreactive Y atoms scattering (i.e., to c.m. angles near $\Theta = 180°$).

In the simulation of the nonreactive Y atom TOFs and laboratory angular distribution (not shown), it was found that the translational energy distribution and c.m. angular distribution are not completely separable. To simulate these data at small laboratory angles corresponding to small c.m. angles (i.e., nearly directly forward-scattered Y atoms), it is necessary to assume a translational energy distribution that is essentially identical to the measured collision energy distribution. This corresponds to nearly elastic scattering of Y atoms off ethane at small c.m. angles. At wider laboratory angles, the nearly elastic $P(E)$ predicts an arrival time that is faster than the experimental data and is too narrow. Thus, the translational energy distribution for larger c.m. angle scattering appears to be much more inelastic. Such behavior is consistent with a larger transfer of initial translational energy into internal (i.e., rotational and vibrational) motion of the scattered products for small impact parameter collisions, since the wider c.m. angle scattering of Y atoms results predominantly from these smaller impact parameter collisions. Simulation of this behavior was achieved by assuming a weighted sum of two pairs of separable $P(E)$ and $T(\Theta)$ distributions; a nearly elastic component for the more forward-scattered Y atoms ($\Theta < 110°$) and a much more inelastic component at larger c.m. angles ($\Theta > 70°$). The simulated TOF spectra in Figure 9 include contribution at all angles from both of these pairs of c.m. distributions, indicated as dashed curves. As expected for nonreactive scattering at this relatively high collision energy, it is not necessary to assume a strong dependence of scattering cross section on initial collision energy; therefore, no threshold collision energy was used in simulating the data for this channel.

Figure 10 shows the product flux in velocity space for nonreactively scattered Y atoms derived from the weighted sum of these c.m distributions. Superimposed on this flux map is the Newton diagram for the most probable beam velocities; note that Y products are scattered beyond the elastic limit for this Newton diagram, since the distribution in beam velocities results in a comparable distribution in nonreactive recoil velocities even for purely elastic collisions. This flux map indicates the strong forward-scattered nature of Y nonreactive scattering, with only a very small fraction of nonreactive Y atoms scattered beyond $\Theta = 90°$. Although the translational energy distribution for a given c.m. angle changes from essentially elastic for small Θ

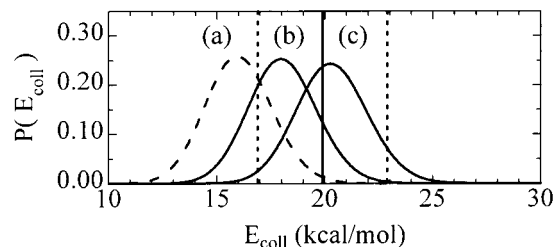**1112** *J. Phys. Chem. A, Vol. 104, No. 6, 2000*

Stauffer et al.
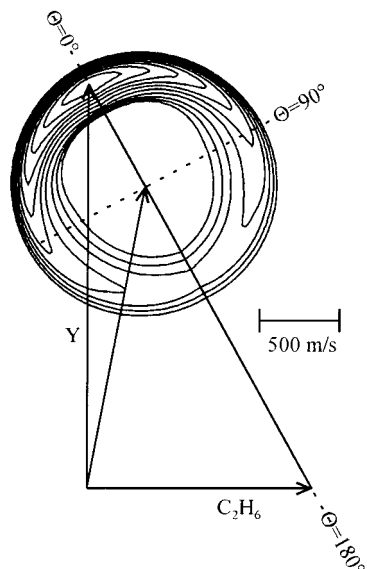
Figure 10. Contour map of Y atom product flux in velocity space. Note that the spacing of the contours is a logarithmic scale, with the forward-scattered inner contour roughly a factor of 170 larger than the outermost contour.

Figure 11. Collision energy distributions for $\langle E_{coll} \rangle$ = (a) 16.1 kcal/mol, (b) 18.1 kcal/mol, and (c) 20.4 kcal/mol data sets. Solid curves correspond to data sets where YH_2 and YC_2H_4 products are observed. Solid vertical line is best estimate of C−H insertion barrier height (19.9 ± 3.0 kcal/mol); dashed vertical lines represent 3.0 kcal/mol error bars.

to quite inelastic for $\Theta = 180°$, the integrated c.m. angular distribution obtained by integrating the total flux as a function of Θ is found to monotonically decay from $\Theta = 0°$ to $\Theta = 180°$.

B. Threshold Behavior for $YH_2 + C_2H_4$ and $YC_2H_4 + H_2$ Product Formation. Studies of the Y + C_2H_6 reaction were carried out at additional collision energies as indicated in Table 1. At all collision energies studied, nonreactive Y atom signal showed behavior quite similar to that at $\langle E_{coll} \rangle$ = 23.0 kcal/mol, with essentially elastic scattering of Y atoms at small angles and somewhat more inelastic scattering at larger c.m. angles. In all cases, the nonreactive angular distribution was found to decrease monotonically to $\Theta = 180°$, with no evidence for a strong contribution from long-lived collision complexes dissociating back to reactants.

At all $\langle E_{coll} \rangle \geq 18.1$ kcal/mol, signal was observed from both YH_2 and YC_2H_4 reaction products, although for the $\langle E_{coll} \rangle$ = 18.1 kcal/mol data set, signal at the c.m angle, $\theta_{c.m.}$, from both of these channels is present but very weak, making it extremely difficult to obtain a complete data set for both channels. To more accurately probe the collision energy dependence of the two products, a slightly higher collision energy, $\langle E_{coll} \rangle$ = 18.5 kcal/mol, was used to fully study the laboratory angular distributions and TOF spectra of products. The reaction cross sections increase rapidly enough through this energy range that sufficient signal-to-noise was obtained at this slightly larger collision energy for both channels in a reasonable amount of time. The best-fit c.m. distributions for both reaction channels are qualitatively quite similar to those shown above for the $\langle E_{coll} \rangle$ = 23.0 kcal/mol data set. The $P(E)$ for the $YH_2 + C_2H_4$ channel peaks at 0.9 ± 0.1 kcal/mol and falls to essentially zero near 8 kcal/mol, whereas the $P(E)$ for the $YC_2H_4 + H_2$ channel reaches a maximum at 1.9 kcal/mol and decays to zero at roughly 17 kcal/mol. Similarly, the c.m. angular distributions found to best simulate these two product channels are essentially identical to those shown in Figure 5 for YH_2 products and Figure 8 for YC_2H_4 products. These c.m. distributions were derived after assuming a threshold collision energy of 19.9 ± 0.5 kcal/mol for both reaction channels. As was the case for the data obtained at $\langle E_{coll} \rangle$ = 23.0 kcal/mol, this threshold energy assumption is

necessary to properly simulate both the arrival times and widths of the individual TOF spectra for both reaction channels and is found to be the same, within the stated uncertainty, for both reaction products. The threshold required for this data set is, however, lower than that required in simulating the higher collision energy data described earlier. Therefore, it is likely that the reaction cross sections for both channels increase quite rapidly through this energy range, and the high-energy tail of a given collision energy distribution dominates the formation of reaction products. This results in an overestimation of the real energetic threshold because a simple step function is assumed to simulate the real cross section behavior. As the high-energy tail of the collision energy distribution approaches the actual energetic threshold for reaction from above, the assumed onset energy used to simulate the data will more closely approach the real energetic threshold.

Additional confirmation of this threshold behavior for both reaction product channels was obtained through several studies at lower collision energies. Shown in Figure 11 are collision energy distributions (nominally $\langle E_{coll} \rangle$ = 16.1, 18.1, and 20.4 kcal/mol) studied near this apparent threshold energy of 19.9 kcal/mol. In all cases, nonreactive scattering of Y atoms off ethane was observed, However, signal from both reactive channels was observed at $\theta_{c.m.}$ only for the two larger collision energies, whereas no signal was observed above the noise at $\langle E_{coll} \rangle$ = 16.1 kcal/mol. It is important to note that these studies were carried out while maintaining the velocity of the yttrium beam near 2130 m/s by using a mixture of 8% Ne in He as a seed gas. Different collision energies were obtained by varying the concentration of C_2H_6 from 10% in H_2 for the highest energy distribution shown in Figure 11 to 40% in H_2 for the lowest collision energy distribution. This allows the intensity of the yttrium beam to remain essentially constant while studying the collision energy behavior. Furthermore, the collision energy is systematically decreased by *increasing* the concentration of ethane in the secondary beam. This allows confirmation that a reduction of YH_2 or YC_2H_4 signal at lower collision energies is not simply due to a smaller number density of reactants in the beam interaction volume. Instead, the behavior at these collision energies is consistent with a threshold for both of these reaction channels of approximately 19.9 kcal/mol.

IV. Discussion

A. Determination of C−H Insertion Barrier. A threshold behavior for product formation is observed for both the $YH_2 + C_2H_4$ and $YC_2H_4 + H_2$ reaction channels. At all collision energies studied, the threshold collision energy necessary to properly fit the experimental data has been determined to be the same within the experimental uncertainty for both channels.

H$_2$ and C$_2$H$_4$ Elimination

J. Phys. Chem. A, Vol. 104, No. 6, 2000 **1113**

From the threshold energy needed to fit the lower collision energy data, this barrier appears to occur at approximately 19.9 kcal/mol and corresponds to the largest barrier along the reactive pathway toward products.

On the basis of the theoretically calculated thermodynamics for this reaction system, the largest barrier along the reaction pathway to both product channels is the initial barrier to C–H insertion. The possibility exists that the largest barrier along the reaction pathway corresponds to a different transition state, e.g., that for β-hydrogen transfer in the insertion intermediate. However, the nonreactive data obtained at all collision energies studied here do not indicate that this is the case. In all these studies, the nonreactive Y atom signal is completely dominated by a forward scattering component, with c.m. angular distributions showing a monotonic decay to $\Theta = 180°$. Such scattering indicates a process that is dictated by a repulsive interaction between the two colliding molecules. Similar behavior was observed recently in our laboratory in collisions of molybdenum atoms with Ne, Ar, and C$_2$H$_6$.[24] The strong forward scattering directly contrasts the behavior seen for crossed molecular beam reactions of transition metal atoms with ethylene[22] and acetylene.[23] In these previous cases, the nonreactive metal atom signal is found to peak strongly at $\Theta = 180°$, indicating formation of collision complexes that persist at least several rotational periods prior to decay back to reactants.[22,23] If any barriers existed after the formation of an initial C–H insertion complex that are comparable to or greater than the barrier to C–H insertion, evidence for decay of long-lived collision complexes would also be evident in the nonreactive data shown here for the Y + C$_2$H$_6$ reaction. Such evidence is, however, not seen. We therefore conclude that the barrier to formation of YH$_2$ + C$_2$H$_4$ and YC$_2$H$_4$ + H$_2$ products corresponds to the initial C–H insertion barrier.

To ascertain the height of this C–H insertion barrier relative to ground-state Y + C$_2$H$_6$, it is important to consider the internal excitation that may be present in the reactants prior to collision. Characterization of the Y beam indicates that some spin–orbit excited-state Y(a^{2}D$_{5/2}$), lying 1.5 kcal/mol above the ground spin–orbit state, is present.[23] Furthermore, although rotations are in general cooled quite efficiently during a supersonic expansion, vibrational excitation is generally not cooled as well. Thus, the vibrational temperature of the ethane in the molecular beam may be as high as room temperature. This will result in population of one or more quanta of primarily low-frequency modes of the ethane, most notably torsion about the C–C bond at 278 cm^{-1}.[42,43] Although, on average, the vibrational energy of ethane at room temperature is roughly 0.4 kcal/mol, greater than 2% of the ethane molecules will have an additional 2.3– 2.7 kcal/mol of internal energy in vibrational modes such as the C–C stretch (944.8 cm^{-1}) or the asymmetric CH$_3$ rock (821.5 cm^{-1}).[42] None of these lower frequency normal modes are expected to be directly along the reaction coordinate for C–H insertion, but this additional excitation may result in insertion and subsequently reaction for a small fraction of collisions despite being below the barrier for insertion into vibrationally cold ethane. Because of these uncertainties in the internal energy of the reactants, in addition to the fact that the 19.9 kcal/mol measurement may slightly overestimate the barrier to formation of reaction products as discussed above, we place conservative error bars on this measurement to derive a 19.9 ± 3.0 kcal/mol barrier for insertion of ground-state Y atoms into ethane.

B. Reaction Product Channels. Above the experimentally determined threshold for C–H insertion, reactive signal is seen for both YH$_2$ + C$_2$H$_4$ and YC$_2$H$_4$ + H$_2$ product channels. Theoretical calculations predict that a relatively stable dihydrido intermediate, (H)$_2$Y(C$_2$H$_4$), exists prior to elimination of molecular hydrogen to form YC$_2$H$_4$.[5] The observation of both of these channels following initial insertion is consistent with decay of this final reaction intermediate. Formation of both product channels thus results from competition between reductive elimination of H$_2$ and elimination of ethylene from this dihydrido intermediate.

The product translational energy distributions for the YH$_2$ + C$_2$H$_4$ channel is found to peak extremely sharply near zero kinetic energy, with a large fraction ($\sim$80% based on the calculated thermodynamics of this channel) of the available energy transferred into internal excitation of the products at all collision energies. This indicates that formation of these products occurs over a negligible exit barrier above the final product energetics or, if a barrier to C$_2$H$_4$ elimination is present, much of the excess energy is channeled into internal degrees of freedom of the recoiling fragments. This latter behavior is likely to occur only in cases where the barrier is "early" along the reaction coordinate and vibrational modes of the recoiling fragments can couple strongly to the reaction coordinate as the fragments dissociate.[44] Such a situation is, however, not likely to be the case here. The dihydrido intermediate contains what is essentially a single bond between the Y atom and the C$_2$H$_4$ ligand, since the valency of Y can only allow three bonds to be formed simultaneously. Calculations demonstrate that the H–H distance in this intermediate is sufficiently long that the bonding between Y and the two H atoms is not a single σ-addition complex but instead two single bonds to the hydrogen atoms.[45] This leaves only a single electron to bind to the ethylene ligand. Thus, the bond that forms is necessarily a π-bonded complex, where the C–C bond distance in the C$_2$H$_4$ ligand is only slightly longer than that of free ethylene, as opposed to a metallacyclopropane complex, where the C–C double bond has been essentially broken.[46] Upon dissociation, it therefore appears unlikely that any barrier along the reaction coordinate would result from, for example, the breaking of two Y–C bonds and re-formation of the C–C double bond of ethylene. An exit channel barrier, if present, should instead result from a repulsive interaction between the nonbonding metal atom electrons and the doubly occupied π-bond of ethylene. Thus, it is not likely that a substantial amount of internal excitation of the dissociating fragments occurs after this final transition state. We therefore conclude from the product $P(E)$ for this channel that little or no barrier exists above the product energetic threshold during dissociation of the dihydrido intermediate. Calculations by Blomberg et al. have shown that bare Y atoms can form relatively strongly bound π-complexes with ethylene while maintaining substantial d^{1}s^2 ground electronic state character,[46] which suggests that the repulsive interaction between ethylene and the ground electronic state of yttrium is not substantial. Furthermore, the addition of two hydride ligands to Y has the effect of removing some of the electron density from the metal atom center,[26,27] further reducing repulsive interactions during the dissociation to form YH$_2$ + C$_2$H$_4$.

The best-fit c.m. angular distributions for the ethylene elimination reaction channel at all collision energies show forward–backward symmetry, consistent with the formation of a long-lived collision complex prior to dissociation to form these products. The peaking of the $T(\Theta)$ at the poles ($\Theta = 0°$, 180°) relative to $\Theta = 90°$ is dictated by the partitioning of the total angular momentum of the collision complex, **J**, between the

final orbital angular momentum of dissociating products, $\mathbf{L'}$, and the internal rotational angular momenta of these products, $\mathbf{j'}$.[38] Because of the relatively large reduced mass of the Y + C_2H_6 reactants coupled with the fact that rotations are efficiently cooled during the supersonic expansion, $\mathbf{J}$ is essentially equal to the initial orbital angular momentum of the colliding partners, $\mathbf{L}$. In cases where all of this initial angular momentum is taken up in $\mathbf{L'}$, corresponding to no rotational excitation of products, $\mathbf{L'}$ is oriented nearly parallel to $\mathbf{L}$ and the relative velocity vector of scattered products is constrained to the same plane as the initial relative velocity vector. This results in a very sharply polarized $T(\Theta)$, peaking at $\Theta = 0°$ and $\Theta = 180°$ for near-prolate collision complexes, with a limiting case of $T(\Theta) = \sin^{-1}(\Theta)$ for $\mathbf{L} = \mathbf{L'}$.[38] Conversely, in cases where rotational excitation of products is quite large, $\mathbf{j'} \approx \mathbf{L}$, and the magnitude of $\mathbf{L'}$ is correspondingly much smaller than that of $\mathbf{L}$. As a result, products are scattered out of the plane perpendicular to the initial $\mathbf{L}$, and the sharp polarization of the $T(\Theta)$ does not occur. In the case of the best-fit $T(\Theta)$ for the $YH_2 + C_2H_4$ products, this polarization is quite evident (Figure 5). Although the polarization is not in the limit that all initial orbital angular momentum is taken up as $\mathbf{L'}$, the $T(\Theta)$ indicates that only a relatively small fraction of the angular momentum of the collision complex is transferred into rotational excitation of the $YH_2 + C_2H_4$ products, and $\mathbf{L'}$ is comparable in magnitude to $\mathbf{L}$ for most collisions.

In contrast to the relatively sharply polarized $T(\Theta)$'s observed for the $YH_2 + C_2H_4$ channel, essentially isotropic c.m. distributions are seen for the H_2 elimination channel at all collision energies above the C−H insertion threshold (Figure 8). Again, the observed forward−backward symmetry is expected given the considerable rearrangement that must occur in the collision complex prior to formation of these products. The negligible polarization of the c.m. distributions indicates that $\mathbf{L}$ and $\mathbf{L'}$ are not strongly coupled for this reaction channel. Because of the small reduced mass of this product channel, the exit orbital angular momentum is constrained to be much smaller in magnitude than $\mathbf{L}$, and a substantial amount of this angular momentum must instead be taken up as rotational excitation of the recoiling fragments.

The translational energy distributions for the H_2 elimination channel peak at kinetic energies roughly twice as large as the most probable translational energies for the $YH_2 + C_2H_4$ channel at all collision energies, with approximately 60−65% of the energy available to products going into internal excitation of the recoiling fragments. As discussed earlier, signal was observed at $m/e = 115$ corresponding either to secondary dissociation of highly internally excited nascent YC_2H_4 products or to fragmentation of YC_2H_4 products during ionization. The translational energy distributions for this channel do show a large degree of product internal excitation; however, in order for a substantial fraction of YC_2H_4 products to undergo secondary dissociation, this would require that essentially all of this internal excitation goes into vibrational excitation of the YC_2H_4 fragment. This is in fact not the case, since some of this internal energy is tied up in the large degree of product rotational excitation for this channel, and we expect that vibrational excitation of H_2 products may also carry away some of this available energy. Furthermore, the ratio of $m/e = 117$ to $m/e = 115$ signal remains constant at all collision energies studied. Thus, signal at $m/e = 115$ appears to result almost exclusively from fragmentation of YC_2H_4 during ionization.

At all collision energies where reaction products have been observed, the peak intensities of the YH_2 TOF spectra are stronger than those for YC_2H_4 at all laboratory angles despite being scattered over a larger range of angles. Assuming comparable ionization cross sections for the two detected products and taking into account the measured degree of fragmentation of YC_2H_4 products to $YC_2H_2^+ + H_2 + e^-$ during ionization, formation of YH_2 products is favored over YC_2H_4 production by more than an order of magnitude at all collision energies. Thus, the decomposition of the $(H)_2Y(C_2H_4)$ intermediate appears to strongly favor the thermodynamically less favorable ethylene elimination over reductive elimination of H_2. This behavior suggests that there may be a slightly larger barrier to H_2 elimination above the final product asymptote than is present for the C_2H_4 elimination channel discussed above. This is consistent with the fact that a somewhat larger fraction of available energy is channeled into translation of the $YC_2H_4 + H_2$ product fragments than is channeled into $YH_2 + C_2H_4$ translation.

Another possible explanation for the dominance of the ethylene elimination channel is that the calculated energetics underestimate the YH_2 binding energy, and this channel is actually more thermodynamically favorable than the $YC_2H_4 + H_2$ channel. However, at all collision energies, the translational energy distributions appear to be quite consistent with the calculated product energetics for both channels depicted in Figure 1, taking into account both the high-energy tail of the collision energy distribution and the high-energy tail of the best-fit $P(E)$. In all cases, the best-fit $P(E)$ falls off to zero at smaller energies for the ethylene elimination channel. On the basis of these fits, there is no evidence that the relative energies of these two product channels are reversed.

In an attempt to model this observed dominance of the C_2H_4 elimination channel over the $YC_2H_4 + H_2$ product channel, we have carried out Rice−Ramsburger−Kassel−Marcus (RRKM) calculations[47] for dissociation from $(H)_2Y(C_2H_4)$. Since extensive ab initio calculations have not been performed to date on the transition states leading to these two competing product channels, we have only carried out crude calculations assuming "loose" transition states for both products. These variational calculations were carried out assuming simple C_6 potentials between the dissociating product molecules, the magnitudes of which were estimated using the polarizabilities of the dissociated products.[34,48] For each transition state, 20 internal degrees of freedom were considered. To estimate the frequencies of internal modes in the transition states, frequencies of the separated fragments were assumed. For the H_2 elimination channel, 15 harmonic modes were included for the YC_2H_4 fragment and one for the H_2 fragment. Vibrational frequencies of the YC_2H_4 moiety were assumed to be identical to those calculated for free ZrC_2H_4.[48] For the C_2H_4 elimination channel, three harmonic modes for YH_2 were estimated and 12 modes were included for C_2H_4.[49] The soft bending vibrations for the two separating moieties with respect to each other as well as torsional rotation about the dissociating axis were treated as free internal rotors for both transition states. We used reasonable estimates of the vibrational frequencies of the $(H)_2Y(C_2H_4)$ complex; however, in calculating the ratio of YH_2 products to YC_2H_4 products, the density of states of this complex cancels out. Assuming an insertion barrier of 19.9 kcal/mol and moments of inertia calculated using an initial C−H insertion transition-state geometry similar to that for Y + CH_4 insertion,[50] the total angular momentum of the reaction complex is limited to $J <$ 150 at $\langle E_{coll} \rangle = 23.0$ kcal/mol; thus, calculations were performed for $J = 0$−150 using the calculated product energetics for the two channels.

H$_2$ and C$_2$H$_4$ Elimination

J. Phys. Chem. A, Vol. 104, No. 6, 2000 **1115**

Under these assumptions, the RRKM calculations carried out for a collision energy of 23.0 kcal/mol predict that the H$_2$ elimination channel should dominate by a factor of 25−130 for all J levels populated. Note that the centrifugal barrier for H$_2$ elimination increases more rapidly with increasing J than does the barrier for C$_2$H$_4$ elimination because of the smaller moments of inertia at the orbiting transition state for dissociation to YC$_2$H$_4$ + H$_2$. However, both product states are energetically accessible for J = 0−150, and dissociation to YC$_2$H$_4$ + H$_2$ still dominates by a factor of 25 for J = 150. The assumption of a loose transition state for H$_2$ elimination therefore substantially overestimates the contribution of this product channel relative to the C$_2$H$_4$ elimination channel. Thus, H$_2$ elimination from (H)$_2$Y(C$_2$H$_4$) appears to traverse a substantially tighter transition state and therefore suggests that at least a small barrier exists above the YC$_2$H$_4$ + H$_2$ product asymptote.

A similar barrier to H$_2$ elimination has been postulated to exist in the Y + C$_2$H$_2$ reaction based on crossed molecular beam experiments carried out previously in our laboratory.[23] In that case, the YC$_2$ + H$_2$ product channel translational energy distribution exhibited a relatively large degree of product translational excitation that directly indicated the existence of an exit channel barrier. This barrier was attributed to a repulsive interaction between the YC$_2$ fragment, which is expected to exhibit substantial closed-shell s^2 character, and the departing H$_2$ fragment.[23] We suspect that a repulsive interaction may also result in a small barrier in the final H$_2$ elimination step of the Y + C$_2$H$_6$ reaction to form YC$_2$H$_4$ products. Calculations have been carried out on several low-lying electronic states of YC$_2$H$_4$, indicating that the ground electronic state of this molecule shows substantial "metallacyclopropane" character; i.e., the C−C π-bond in the ethylene moiety is essentially broken.[46] This ground state is found to mix in substantial yttrium excited state d^{2}s^1 character in forming the metallocyclopropane. Additionally, a low-lying excited state of YC$_2$H$_4$ has also been found, nearly isoenergetic to the ground state, which mixes in predominantly the ground state d^{1}s^2 configuration of yttrium. This excited state exhibits a shorter C−C bond and a longer Y−C$_2$H$_4$ distance than the metallacyclopropane state and is better described as a Y−C$_2$H$_4$ π-bonded complex.[46] This type of bonding is quite similar to that found in the (H)$_2$Y(C$_2$H$_4$) intermediate, as indicated by the nearly identical geometry of the YC$_2$H$_4$ moiety in the intermediate.[45] As discussed above, this π-bonding is necessary in the intermediate because of the lack of sufficient valence electrons of yttrium to form four bonds. Thus, if dissociation of the dihydrido intermediate occurs to form the π-bonded yttrium−ethylene complex by maintaining the YC$_2$H$_4$ bonding present in the intermediate, a small exit channel barrier may result from a repulsive interaction between the dissociating H$_2$ and the predominantly s^2 closed-shell YC$_2$H$_4$ fragments.

If, on the other hand, the final yttrium ethylene product formed following H$_2$ elimination is the ground-state metallacyclopropane, the dominant electronic configuration of the metal fragment will have s^1 character,[46] and the repulsive interaction with the H$_2$ σ-bond due to the electronic configuration at the metal atom center will be reduced during dissociation. However, substantial rearrangement of the electronic configuration of the YC$_2$H$_4$ moiety must occur during dissociation to form the metallacyclopropane, possibly resulting in a tight transition state and small exit barrier for the H$_2$ elimination channel. Of course, further ab initio calculations on the nature of the transition state for H$_2$ elimination would be enlightening.

C. Possibility of C−C Insertion. We note finally that the barrier for insertion of Y into the C−C bond of ethane has been calculated to lie 28.5 kcal/mol above the reactant asymptote.[5] At the highest collision energy studied here, a substantial fraction of collisions are able to surmount this calculated threshold. Following C−C insertion, rearrangement may occur to ultimately form YCH$_2$ + CH$_4$ reaction products, expected to lie energetically below the C−C insertion barrier. The experiments reported here have focused only on detection of products that are formed following C−H insertion. Detection of YCH$_2$ is complicated slightly by the fact that the c.m. angle for this highest collision energy study lies quite close to the Y atom beam, which additionally contains a small amount of YO contamination. Because of the similarity in mass between YO (m/e = 105) and YCH$_2$ (m/e = 103) as well as the fact that signal from this reaction channel is expected to be substantially weaker than, for example, the YH$_2$ data reported here, additional steps are presently being taken to remove YO contaminant from the atomic beam. Therefore, the characterization of possible C−C insertion reactions by Y atoms at high collision energies is reserved for future studies.

V. Conclusions

Two distinct product channels, YH$_2$ + C$_2$H$_4$ and YC$_2$H$_4$ + H$_2$, are observed following reactions between ground-state yttrium atoms and ethane at high collision energies ($\langle E_{coll} \rangle \geq$ 18.1 kcal/mol). At lower collision energies, only nonreactive Y + C$_2$H$_6$ collisions are found to occur, with no evidence for a substantial fraction of collisions undergoing C−H insertion prior to decay back to reactants. A collision energy threshold behavior is observed for both reaction product channels, indicating that the high-energy tail of the collision energy distribution dominates the formation of reaction products. Studies at several collision energies allow determination of the barrier to C−H insertion of Y atoms into ethane, found to lie 19.9 ± 3.0 kcal/mol above ground-state reactants. This compares well with the calculated barrier of 20.7 kcal/mol for insertion of Y atoms into methane.[5]

At all collision energies above the C−H insertion threshold, the YH$_2$ + C$_2$H$_4$ product channel is found to dominate the second channel, i.e., H$_2$ elimination from a common (H)$_2$Y-(C$_2$H$_4$) intermediate, by greater than an order of magnitude. Products of the C$_2$H$_4$ elimination channel exhibit only a small fraction of available energy in the relative translation of the scattering fragments, instead indicating a large degree of internal excitation. This behavior is consistent with a C$_2$H$_4$ elimination mechanism in which little or no barrier exists above the final YH$_2$ + C$_2$H$_4$ asymptote. Product translational energy distributions for the H$_2$ elimination channel also exhibit a large degree of internal excitation of products, although a larger fraction of energy available to products is transferred into relative translation. The dominant nature of the YH$_2$ product channel suggests that a tighter transition state exists for H$_2$ elimination than for elimination of C$_2$H$_4$ from the common dihydrido intermediate.

References and Notes

(1) Ritter, D.; Weisshaar, J. C. *J. Am. Chem. Soc.* **1990**, *112*, 6425.

(2) Ritter, D.; Carroll, J. J.; Weisshaar, J. C. *J. Phys. Chem.* **1992**, *96*, 10636.

(3) Carroll, J. J.; Weisshaar, J. C. *J. Am. Chem. Soc.* **1993**, *115*, 800.

(4) Carroll, J. J.; Haug, K. L.; Weisshaar, J. C. *J. Am. Chem. Soc.* **1993**, *115*, 6962.

(5) Carroll, J. J.; Haug, K. L.; Weisshaar, J. C.; Blomberg, M. R. A.; Siegbahn, P. E. M.; Svensson, M. *J. Phys. Chem.* **1995**, *99*, 13955.

(6) Carroll, J. J.; Weisshaar, J. C.; Siegbahn, P. E. M.; Wittborn, C. A. M.; Blomberg, M. R. A. *J. Phys. Chem.* **1995**, *99*, 14388.

(7) Carroll, J. J.; Weisshaar, J. C. *J. Phys. Chem.* **1996**, *100*, 12355.

(8) Wen, Y.; Yethiraj, A.; Weisshaar, J. C. *J. Chem. Phys.* **1997**, *106*, 5509.

(9) Senba, K.; Matsui, R.; Honma, K. *J. Phys. Chem.* **1995**, *99*, 13992.

(10) Honma, K. *Phys. Chem. Chem. Phys.* **1999**, *1*, 3235.

(11) Lian, L.; Mitchell, S. A.; Rayner, D. M. *J. Phys. Chem.* **1994**, *98*, 11637.

(12) Parnis, J. M.; Lafleur, R. D.; Rayner, D. M. *J. Phys. Chem.* **1995**, *99*, 673.

(13) Campbell, M. L. *J. Am. Chem. Soc.* **1997**, *119*, 5984.

(14) McClean, R. E.; Campbell, M. L.; Kölsch, E. J. *J. Phys. Chem. A* **1997**, *101*, 3348.

(15) Campbell, M. L. *J. Phys. Chem. A* **1997**, *101*, 9377.

(16) Campbell, M. L. *J. Phys. Chem. A* **1998**, *102*, 892.

(17) Campbell, M. L. *J. Chem. Soc., Faraday Trans.* **1998**, *94*, 353.

(18) Mitchell, S. A.; Hackett, P. A. *J. Chem. Phys.* **1990**, *93*, 7822.

(19) Brown, C. E.; Mitchell, S. A.; Hackett, P. A. *Chem. Phys. Lett.* **1992**, *191*, 175.

(20) Blitz, M. A.; Mitchell, S. A.; Hackett, P. A. *J. Phys. Chem.* **1991**, *95*, 8719.

(21) Wen, Y.; Porembski, M.; Ferrett, T. A.; Weisshaar, J. C. *J. Phys. Chem. A* **1998**, *102*, 8362.

(22) Willis, P. A.; Stauffer, H. U.; Hinrichs, R. Z.; Davis, H. F. *J. Phys. Chem. A* **1999**, *103*, 3706.

(23) Stauffer, H. U.; Hinrichs, R. Z.; Willis, P. A.; Davis, H. F. *J. Chem. Phys.* **1999**, *111*, 4101.

(24) Hinrichs, R. Z.; Willis, P. A.; Stauffer, H. U.; Schroden, J. J.; Davis, H. F. *J. Chem. Phys.*, in press.

(25) Willis, P. A.; Stauffer, H. U.; Hinrichs, R. Z.; Davis, H. F. *J. Chem. Phys.* **1998**, *108*, 2665.

(26) Balasubramanian, K.; Ravimohan, C. *Chem. Phys. Lett.* **1988**, *145*, 39.

(27) Siegbahn, P. E. M. *Theor. Chim. Acta* **1994**, *87*, 441.

(28) Crabtree, R. H. *The Organometallic Chemistry of the Transition Metals*; John Wiley & Sons: New York, 1994.

(29) (a) Bergman, R. G. *J. Organomet. Chem.* **1990**, *400*, 273. (b) Arndtsen, B. A.; Bergman, R. G.; Mobley, T. A.; Peterson, T. H. *Acc. Chem. Res.* **1995**, *28*, 154. (c) Shilov, A. E.; Shul'pin, G. B. *Chem. Rev.* **1997**, *97*, 2879. (d) Koga, N.; Morokuma, K. *Chem. Rev.* **1991**, *91*, 823.

(30) Siegbahn, P. E. M.; Blomberg, M. R. A. In *Theoretical Aspects of Homogeneous Catalysis*; van Leeuwen, P. W. N. M., Morokuma, K., van Lenthe, J. H., Eds.; Kluwer: Dordrecht, 1995; pp 15−63.

(31) Blomberg, M. R. A.; Siegbahn, P. E. M.; Svensson, M. *J. Am. Chem. Soc.* **1992**, *114*, 6095.

(32) Wittborn, A. M. C.; Costas, M.; Blomberg, M. R. A.; Siegbahn, P. E. M. *J. Chem. Phys.* **1997**, *107*, 4318.

(33) Willis, P. A.; Stauffer, H. U.; Hinrichs, R. Z.; Davis, H. F. *Rev. Sci. Instrum.* **1999**, *70*, 2606.

(34) *CRC Handbook of Chemistry and Physics*, 75th ed.; Lide, D. R., Ed.; CRC Press: Boca Raton, FL, 1995.

(35) Koga, N.; Obara, S.; Kitaura, K.; Morokuma, K. *J. Am. Chem. Soc.* **1985**, *107*, 7109.

(36) Powers, D. E.; Hansen, S. G.; Geusic, M. E.; Puiu, A. C.; Hopkins, J. B.; Dietz, T. G.; Duncan, M. A.; Langridge-Smith, P. R. R.; Smalley, R. E. *J. Phys. Chem.* **1982**, *86*, 2556.

(37) Proch, D.; Trickl, T. *Rev. Sci. Instrum.* **1989**, *60*, 713.

(38) Miller, W. B.; Safron, S. A.; Herschbach, D. R. *Discuss. Faraday Soc.* **1967**, *44*, 108.

(39) Miller, W. B.; Safron, S. A.; Herschbach, D. R. *J. Chem. Phys.* **1972**, *56*, 3581.

(40) Parson, J. M.; Lee, Y. T. *J. Chem. Phys.* **1972**, *56*, 4658.

(41) Levine, R. D.; Bernstein, R. B. *Molecular Reaction Dynamics and Chemical Reactivity*; Oxford University Press: Oxford, 1987; p 412−417.

(42) Herzberg, G. *Molecular Spectra and Molecular Structure, Vol. 2: Infrared and Raman Spectra of Polyatomic Molecules*; Van Nostrand: New York, 1945; p 343−346.

(43) Herzberg, G. *Molecular Spectra and Molecular Structure, Vol. 3: Electronic Spectra and Electronic Structure of Polyatomic Molecules*; Van Nostrand: New York, 1966; p 646.

(44) Polanyi, J. C. *Acc. Chem. Res.* **1972**, *5*, 161.

(45) Siegbahn, P. E. M. *J. Am. Chem. Soc.* **1993**, *115*, 5803.

(46) Blomberg, M. R. A.; Siegbahn, P. E. M.; Svensson, M. *J. Phys. Chem.* **1992**, *96*, 9794.

(47) Zhu, L.; Hase, W. L. Program 644, Quantum Chemistry Program Exchange, Indiana University.

(48) Carroll, J. J. Ph.D. Thesis, University of Wisconsin−Madison, 1995.

(49) Chase, M. W., Jr.; Davies, C. A.; Downey, J. R.; Frurip, D. J.; McDonald, R. A.; Syverud, A. N. JANAF Thermochemical Tables. *J. Phys. Chem. Ref. Data* **1981**, *13* (Suppl. 1)

(50) Siegbahn, P. E. M.; Blomberg, M. R. A.; Svensson, M. *J. Am. Chem. Soc.* **1993**, *115*, 1952.